# Macromolecules in nonhomogeneous velocity gradient fields. II

James H. Aubert, Stephen Prager, and Matthew Tirrell

Citation: The Journal of Chemical Physics **73**, 4103 (1980); doi: 10.1063/1.440597
View online: http://dx.doi.org/10.1063/1.440597
View Table of Contents: http://scitation.aip.org/content/aip/journal/jcp/73/8?ver=pdfcov
Published by the AIP Publishing

# Macromolecules in nonhomogeneous velocity gradient fields. II

James H. Aubert, Stephen Prager, and Matthew Tirrell[a)]

*Departments of Chemical Engineering, Materials Science, and Chemistry, University of Minnesota, Minneapolis, Minnesota 55455*
(Received 24 June 1980; accepted 7 July 1980)

Bead-spring model macromolecules in nonhomogeneous flows migrate relative to the local solvent velocity at the center of mass. We show that this is the result of the net viscous forces acting on all the beads. The analogy between these results and continuum mechanical results on suspensions of neutrally buoyant rigid particles is discussed. Detailed comparisons of this model with the available experimental data in the concentric cone geometry is made. Models with linear springs are found to over-predict the migration somewhat, but all qualitative features of the phenomenon are well represented. This provides a new means of testing macromolecular models.

## I. INTRODUCTION

Bead-spring kinetic theory modeling of macromolecular transport properties in dilute solution is now well developed.[1] A particularly interesting recent prediction of this theory applied to nonhomogeneous flows is that of macromolecular migration.[2] Migration here implies that a suspended particle or macromolecule moves or drifts relative to the solvent velocity at its center of mass, when its motion is observed over a period of time that is long compared to the time scale of Brownian motion. A general analysis of the migration phenomenon will be presented in Sec. II of this paper. This is a generalization of some results given previously on the migration of macromolecules in specific flows.[2] Dill and Zimm[3,4] have recently completed an ingenious set of experiments that demonstrate the macromolecular migration phenomenon in the nonhomogeneous flow set up in a DNA solution confined between rotating concentric cones. They attribute the radial migration of DNA to a radial component of the entropic springlike force, which is predicted for randomly coiling macromolecules.[5] However, the entropic spring force is an intramolecular force, and as shown in Sec. II, cannot result in the motion of the macromolecular center of mass. The analysis of Sec. II also shows that a quasi-thermodynamic argument (for example, see Refs. 6 and 7), that macromolecules migrate to where they are minimally stretched is not justified. Instead, the migration is shown to result from viscous drag with the solvent and to occur only because the flow is nonhomogeneous. Section III of the paper looks at the predicted migration in the concentric cone flow. In Sec. IV we calculate the transient concentration profiles caused by the radial migration, and Sec. V compares the theoretical predictions to the experimental results obtained by Dill and Zimm.

The main goal of this paper is to demonstrate the physics and generality of the migration phenomenon. For this reason we have opted to study the simple linear, elastic (zero-rest-length) dumbbell model, rather than more complex macromolecular models. In doing so, we give up some ability to make quantitatively accurate predictions, but gain (by the mathematical simplicity of the model) the ability to make the physics of the migration phenomenon clear and readily connectable with some other results on suspensions of rigid particles. This migration phenomenon provides an additional and independent way of scrutinizing proposed macromolecular models.

## II. GENERAL TREATMENT OF BEAD-SPRING MODELS IN NONHOMOGENEOUS FLOWS

The macromolecular model we choose to study is shown in Fig. 1. The dumbbell model consists of two beads of equal mass connected by a linear spring. The two beads represent the mass of the macromolecule, and the spring represents the entropic springlike force predicted statistically for a random coiling macromolecule.[5] The important aspect of the model for our present purposes is the fact that the mass of the macromolecule is distributed over large distances relative to the size of a solvent molecule.

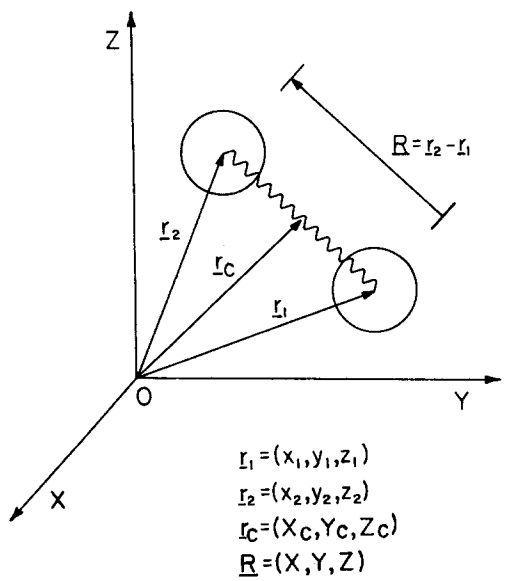


FIG. 1. Elastic dumbbell, made up of two beads connected by a Hookean spring.

a)To whom correspondence should be addressed.

 0021-9606/80/204103-10$01.00  

Each bead of the model experiences forces due to the spring, viscous interaction with the surrounding Newtonian solvent and random Brownian motion forces. The starting point for bead-spring kinetic theory is a force balance written about each of the two beads (acceleration force assumed negligible):

$$0 = -\xi[\dot{\mathbf{r}}_i - \mathbf{v}(\mathbf{r}_i)] - kT\frac{\partial}{\partial \mathbf{r}_i}\ln\Psi + \mathbf{F}_i\,, \quad i = 1, 2\,. \tag{1}$$

The first term is the frictional force, equal to a friction coefficient $\xi$ multiplied by the difference between the bead velocity $\dot{\mathbf{r}}_i$ and the undistributed solvent velocity at that bead's position $\mathbf{v}(\mathbf{r}_i)$. The second term is the Brownian motion force. $\Psi(\mathbf{r}_1, \mathbf{r}_2, t)$ is the configurational distribution function of bead positions, $\Psi(\mathbf{r}_1, \mathbf{r}_2, t)\,d\mathbf{r}_1\,d\mathbf{r}_2$ being equal to the probable number of dumbbells within the configuration space $d\mathbf{r}_1\,d\mathbf{r}_2$. The third term is the spring force, taken to be Hookean; $\mathbf{F}_1 = -\mathbf{F}_2 = H(\mathbf{r}_2 - \mathbf{r}_1)$.

The configurational distribution function satisfies the following equation of continuity in the six-dimensional configurational space:

$$\frac{\partial\Psi}{\partial t} = -\sum_{i=1}^{2}\frac{\partial}{\partial \mathbf{r}_i}\cdot(\dot{\mathbf{r}}_i\cdot\Psi) \tag{2}$$

and must satisfy the symmetry condition, $\Psi(\mathbf{r}_1, \mathbf{r}_2, t) = \Psi(\mathbf{r}_2, \mathbf{r}_1, t)$, and the boundary condition, $\Psi \to 0$ as $(\mathbf{r}_2 - \mathbf{r}_1) \to \pm\infty$.

It is more convenient to use the center-of-mass coordinates and internal coordinates:

$$\mathbf{r}_c = \tfrac{1}{2}(\mathbf{r}_1 + \mathbf{r}_2)\,; \quad \mathbf{R} = (\mathbf{r}_2 - \mathbf{r}_1)\,. \tag{3}$$

The configurational distribution function can be written equivalently in terms of these coordinates, $\Psi(\mathbf{r}_c, \mathbf{R}, t)$. If one is interested in the migration of macromolecules relative to solvent, it is sufficient to calculate the center-of-mass concentration of dumbbells. The center of mass concentration is obtained from $\Psi$ by:

$$C(\mathbf{r}_c, t) = \int_{-\infty}^{+\infty}\Psi(\mathbf{r}_c, \mathbf{R}, t)\,d\mathbf{R}\,, \tag{4}$$

where it is to be understood that the integration occurs over all internal coordinates.

If the bead velocities, $\dot{\mathbf{r}}_i$, are obtained from Eq. (1), substituted into Eq. (2) and rewritten in terms of internal and center-of-mass coordinates, then the resulting equation can be similarly integrated over internal coordinates to yield a continuity equation for the center-of-mass concentration:

$$\frac{\partial C}{\partial t} + \nabla\cdot[\tfrac{1}{2}C\langle\mathbf{v}(\mathbf{r}_1) + \mathbf{v}(\mathbf{r}_2)\rangle] = D\nabla^2 C\,. \tag{5}$$

The brackets refer to an average over internal coordinates,

$$\langle x\rangle = \int_{-\infty}^{+\infty} x\Psi(\mathbf{r}_c, \mathbf{R}, t)\,d\mathbf{R}\,,$$

and the macromolecular diffusion coefficient $D$ is identified as $kT/2\xi$. (The corresponding continuity equation for single-bead concentration, rather than center-of-mass concentration, is developed in Appendix A. We note here the rather surprising conclusion of Appendix A that, while both distributions do exhibit the effects we are discussing, the time evolution of the effects in the single-bead distribution function is slower.)

Equation (5) differs from the continuity equation derived from continuum mechanics for low molecular weight species in one important aspect. The convective term contains the average undisturbed solvent velocity at the two bead positions rather than the undisturbed solvent velocity at the center of mass of the dumbbell. As is shown below, this difference can lead to a coupling between the center-of-mass motion and the nonhomogeneous contributions to the velocity gradient field.

Consider the following Taylor series expansion for the velocity field at a point $\mathbf{r}$ in terms of an origin 0 at the center of mass of a particular dumbbell:

$$\mathbf{v}(\mathbf{r}) = \mathbf{v}_0 + \mathbf{r}\cdot(\nabla\mathbf{v})_0 + \tfrac{1}{2}\mathbf{rr}:(\nabla\nabla\mathbf{v})_0 + \cdots\,. \tag{6}$$

For homogeneous flows, the last and all higher-order terms are zero. Substituting from Eq. (6) for $\mathbf{v}(\mathbf{r}_1)$ and $\mathbf{v}(\mathbf{r}_2)$ enables one to write

$$\tfrac{1}{2}\langle\mathbf{v}(\mathbf{r}_1) + \mathbf{v}(\mathbf{r}_2)\rangle = \mathbf{v}_0 + \tfrac{1}{8}\langle\mathbf{RR}\rangle:(\nabla\nabla\mathbf{v})_0 + \tfrac{1}{384}\langle\mathbf{RRRR}\rangle\vdots(\nabla\nabla\nabla\nabla\mathbf{v})_0 + \cdots\,. \tag{7}$$

Making this substitution into Eq. (5) yields

$$\frac{\partial C}{\partial t} + \nabla\cdot(C\mathbf{v}_0) + \nabla\cdot[C(\tfrac{1}{8}\langle\mathbf{RR}\rangle:(\nabla\nabla\mathbf{v})_0 + \tfrac{1}{384}\langle\mathbf{RRRR}\rangle\vdots(\nabla\nabla\nabla\nabla\mathbf{v})_0 + \cdots)] = D\nabla^2 C\,. \tag{8}$$

This can be written equivalently as

$$\frac{\partial C(\mathbf{r}_c)}{\partial t} + \nabla\cdot(\mathbf{C}(\mathbf{r}_c)\mathbf{v}(\mathbf{r}_c)) + \nabla\cdot\mathbf{J}^{nh} = D\nabla^2 C(\mathbf{r}_c)\,, \tag{9}$$

where $C(\mathbf{r}_c)$ is the local center-of-mass concentration, $\mathbf{v}(\mathbf{r}_c)$ is the undisturbed solvent velocity field, and $\mathbf{J}^{nh}$ is an "extra" flux of dumbbells that can occur only in a nonhomogeneous velocity field. Specifically for the dumbbell model:

$$\mathbf{J}^{nh} = C(\mathbf{r}_c)[\tfrac{1}{8}\langle\mathbf{RR}\rangle:(\nabla\nabla\mathbf{v})_0 + \tfrac{1}{384}\langle\mathbf{RRRR}\rangle\vdots(\nabla\nabla\nabla\nabla\mathbf{v})_0 + \cdots]\,. \tag{10}$$

Similar arguments show that for the Rouse model with $N$ beads:

$$\mathbf{J}^{nh} = C(\mathbf{r}_c)\left(\frac{1}{2N}\sum_{i=1}^{N}\langle\mathbf{R}_i\mathbf{R}_i\rangle:(\nabla\nabla\mathbf{v})_0 + \frac{1}{24N}\sum_{i=1}^{N}\langle\mathbf{R}_i\mathbf{R}_i\mathbf{R}_i\mathbf{R}_i\rangle\vdots(\nabla\nabla\nabla\nabla\mathbf{v})_0 + \cdots\right), \tag{11}$$

where $\mathbf{R}_i$ is the vector from the center of mass to the $i$th bead. Note that in compliance with Curie's theorem, only fields of odd tensorial order contribute to the mass flux. We see, as before,[2] that in rectilinear flow there is no net flux across streamlines. We could write Eqs. (10) and (11) equivalently as:

$$\mathbf{J}^{nh} = C(\mathbf{r}_c)\mathbf{v}^{\mathrm{drift}}\,, \tag{12}$$

where the mean drift velocity is $\mathbf{v}^{\mathrm{drift}} = \langle\dot{\mathbf{r}}_c - \mathbf{v}(\mathbf{r}_c)\rangle$. The drift velocity is seen to arise solely from viscous drag

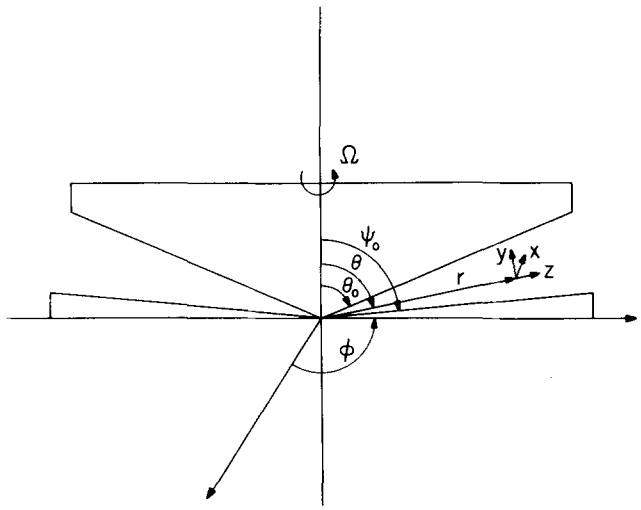


FIG. 2. Schematic of an apparatus capable of producing the rotating concentric cone flow.

forces. The spring forces acting on the two beads (being internal forces) must always sum to zero.

It is interesting to compare these results to some continuum mechanical results on the motions of neutrally buoyant solid particles in low Reynolds number flows. Brenner[8] has derived an expression for the drift velocity of an ellipsoidal particle immersed in an arbitrary Stokes flow $\mathbf{v}$:

$$\mathbf{v}^{\text{drift}}_{\text{ellipsoid}} = \frac{1}{3!}(D^2\mathbf{v})_0 + \frac{1}{5!}(D^4\mathbf{v})_0 + \cdots , \tag{13}$$

where the operator $D^2 = a_1^2(\partial^2/\partial x_1^2) + a_2^2(\partial^2/\partial x_2^2) + a_3^2(\partial^2/\partial x_3^2)$, $a_1$, $a_2$, and $a_3$ are the lengths of the semiaxes of the ellipsoid, and $(x_1, x_2, x_3)$ being body-fixed Cartesian coordinates measured along the principal axes of the ellipsoid. The ellipsoid is predicted to migrate in all nonhomogeneous flows. Hence, it is not surprising to see a similar prediction for macromolecules in nonhomogeneous flows.

For a sphere (of radius $a$), Brenner's, equation becomes

$$\mathbf{v}^{\text{drift}}_{\text{sphere}} = \tfrac{1}{6}a^2(\nabla^2\mathbf{v})_0 . \tag{14}$$

In Stokes flow, the Laplacian of the velocity field is related to the pressure gradient by:

$$\nabla^2\mathbf{v} = -(1/\mu)\nabla P . \tag{15}$$

Hence, the drift velocity may be interpreted as arising from a pressure gradient in the undisturbed Stokes flow.

For plane Poiseuille flow in a channel of width $2B$ [$\mathbf{v} = v_M(1 - 4z^2/B^2)\delta_x$],[9] we have shown[2] that Eq. (10) leads to the result

$$\mathbf{v}^{\text{drift}}_{\text{dumbbell}} = -v_M \frac{\langle R^2\rangle_0}{3B^2}\delta_x , \tag{16}$$

where $\langle R^2\rangle_0$ is the equilibrium mean square end-to-end distance of the dumbbell. Thus the dumbbell lags the undisturbed solvent velocity at its center of mass. We note with interest that if one equates the equilibrium root-mean-square end-to-end distance of the dumbbell with the diameter of a sphere, then Eqs. (14) and (16) give identical results. The macromolecular continuity equation [Eq. (9)] can be used in a range of molecular sizes, from small molecules (for which the predicted drift is zero) to large molecules that can be modeled as rigid particles.

## III. ROTATING CONCENTRIC CONE FLOW

Some curvilinear flows can produce cross-streamline migration. The velocity field to be studied is that of a Newtonian fluid confined between concentric cones, with the top cone rotating with an angular velocity $\Omega$. A schematic of an apparatus capable of producing such a flow is shown in Fig. 2. The velocity field is given by

$$\mathbf{v} = \Omega r\sin\theta \left(1 - \frac{\dfrac{\cos\theta_0}{\sin^2\theta_0} - \dfrac{\cos\theta}{\sin^2\theta} + \displaystyle\int_{\theta_0}^{\theta}\frac{d\theta}{\sin\theta}}{\dfrac{\cos\theta_0}{\sin^2\theta_0} - \dfrac{\cos\Psi_0}{\sin^2\Psi_0} + \displaystyle\int_{\theta_0}^{\Psi_0}\frac{d\theta}{\sin\theta}}\right)\delta_\phi . \tag{17}$$

This velocity field is clearly nonhomogeneous, since the rate of deformation tensor varies spatially:

$$[\nabla\mathbf{v} + (\nabla\mathbf{v})^T] = \left(\frac{-2\Omega/\sin^2\theta}{\dfrac{\cos\theta_0}{\sin^2\theta_0} - \dfrac{\cos\Psi_0}{\sin^2\Psi_0} + \displaystyle\int_{\theta_0}^{\Psi_0}\frac{d\theta}{\sin\theta}}\right)(\delta_\theta\delta_\phi + \delta_\phi\delta_\theta) .$$

It is convenient to define a local Cartesian coordinate frame centered at the center of mass of a particular dumbbell, with its $z$ axis oriented radially, the $x$ axis oriented parallel to the $\phi$ direction, and the $y$ axis oriented parallel to the $\theta$ direction (Fig. 2). It is then possible to calculate the local velocity field in Cartesian coordinates relative to this coordinate frame. If we make the assumptions that the cone angles are near $\frac{1}{2}\pi$ and the dumbbell center of mass is far away from the apex, i.e.,

$$\theta_0 \sim \Psi_0 \sim \tfrac{1}{2}\pi , \tag{19a}$$

$$\frac{\langle R^2\rangle_0}{r_c^2} \ll 1 , \tag{19b}$$

then the $z$-component of the velocity field can be expressed approximately by:

$$v_z \doteq -\frac{\Omega}{\beta_0}\frac{xy}{r_c} - \Omega x\left(1 - \frac{\dfrac{\cos\theta_0}{\sin^2\theta_0} - \dfrac{\cos\theta_c}{\sin^2\theta_c} + \theta_c - \theta_0}{2\beta_0}\right) . \tag{20}$$

In this equation $\beta_0$ is equal to the gap angle, $\Psi_0 - \theta_0$, and the subscript $c$ refers to the center-of-mass position. The nonhomogeneous nature of this velocity field becomes apparent in the first term of Eq. (20). By application of Eq. (12), we find that the radial drift velocity is given by

$$v_r^{\text{drift}} \doteq -\frac{\Omega}{\beta_0 r_c}\frac{\langle XY\rangle}{4} . \tag{21}$$

A similar expression is easily obtained for the drift velocity in the $\phi$ direction, but because of angular sym-

metry, this drift velocity would not be observed as a concentration profile. There is no predicted drift velocity in the $\theta$ direction, since there is no component of velocity in that direction.

Application of Eq. (21) requires evaluation of the average, $\langle XY \rangle$, which in turn requires a complete solution for the configurational distribution function, $\Psi(\mathbf{r}_c, \mathbf{R}, t)$. A complete solution has been obtained for only a small number of simple flows.[1] An approximate evaluation of $\langle XY \rangle$ can be obtained by assuming the average dumbbell dimensions are the same as if the dumbbell were in a locally homogeneous velocity field, with a shear rate equal to the shear rate at the center of mass. This approximation was shown in our first paper to be excellent for the dumbbell in all quadratic flows.[2] Since the shear rate in the apparatus varies little under the assumptions of Eq. (19), we can approximate $\langle XY \rangle$ by the homogeneous shear flow result[1]:

$$\langle XY \rangle \doteq \frac{\langle R^2 \rangle_0}{3} \frac{\Omega}{\beta_0} \tau \ . \tag{22}$$

The shear rate is approximately $\Omega/\beta_0$, consistent with Eqs. (18) and (19), and $\tau$ is the dumbbell relaxation time given by $\xi/4H$. More accurate approximations could be made, but they would be of secondary importance and unwarranted since Eq. (21) is already approximate.

The dumbbells are then predicted to migrate toward the apex of the cones with a drift velocity given by

$$v_r^{\text{drift}} \doteq -\frac{\alpha D}{r} \ , \tag{23}$$

where $\alpha = \langle R \rangle_0^2 \Omega^2 \tau / 12 \beta_0^2 D$. An important point to realize is that this drift velocity is the result of viscous drag and occurs only because the velocity gradients vary spatially. The intramolecular spring forces do nothing more than determine the average size of the dumbbell in response to the local velocity gradient conditions. They can not drive the macromolecule anywhere. As is clear from the connection of this work with Brenner's[8] on rigid particles, flexibility is not a prerequisite for this cross-streamline motion.

## IV. PREDICTED CONCENTRATION PROFILES

With the expression for the radial drift velocity, the time evolution of radial concentration profiles can be obtained from the continuity equation [Eq. (8)] and appropriate boundary conditions. The profiles must satisfy a no-flux condition at the outer solution boundary and at the apex of the cones. In the experiments performed by Dill,[3,4] to which we will compare our predictions, the bottom cone was truncated by intersecting an efflux tube with the bottom cone. The efflux tube was used to drain the solution from the gap. Hence, the inner boundary condition is taken as a no-flux condition at the radius where the efflux tube intersects the bottom cone. This has virtually no effect on the concentration profile beyond a few efflux tube diameters.

The nondimensional problem then takes the form

$$\frac{\partial C}{\partial t} = \frac{1}{r^2} \frac{\partial}{\partial r} \left( r^2 \frac{\partial C}{\partial r} + \alpha r C \right), \quad \text{Initial condition at } t = 0 \quad C = 1 \quad a \le r \le 1$$

$$\text{Boundary conditions at } r = a \quad \text{no flux} \quad r^2 \frac{\partial C}{\partial r} + \alpha r C = 0$$

$$\text{at } r = 1 \quad \text{no flux} \quad r^2 \frac{\partial C}{\partial r} + \alpha r C = 0 \ . \tag{24}$$

The equations have been nondimensionalized via

$$C = \bar{C}/C_0 \ , \quad r = \bar{r}/R_0 \ , \quad a = R_i/R_0 \ , \quad t = \bar{t}D/R_0^2 \ , \tag{25}$$

where the quantities with overbars are dimensional, $C_0$ is the initial uniform macromolecular concentration, $R_0$ is the radius up to which solution fills the gap between the cones, and $R_i$ is the radius at which the efflux tube intersects the bottom cone (which is very small, so that the volume occupied from the radial position $r = 0$ to $r = R_i$ can be neglected).

The steady state concentration profile is obtained by applying the no-flux condition to all radial positions:

$$r^2 \frac{\partial C}{\partial r} + \alpha r C = 0 \ . \tag{26}$$

The solution is given by $C(r) = K r^{-\alpha}$, where $K$ is a normalization factor, given by

$$K = \frac{\int_a^1 r^2 \, dr}{\int_a^1 r^{-\alpha} r^2 \, dr} \tag{27}$$

$$K = (3 - \alpha)(1 - a^3)/(3 - 3a^{3-\alpha}) \ , \quad \text{for } \alpha \neq 3$$

$$K = (a^3 - 1)/3 \ln a \ , \quad \text{for } \alpha = 3 \ .$$

Figure 3 shows a number of steady state concentration profiles for different values of $\alpha$. For values of $\alpha$ greater than 3, the steady state is nearly total migration of the macromolecules to the apex. It must be kept in mind that the bead-spring theory was developed for dilute solutions only. When the solution concentration increases greatly one may expect behavior qualitatively different from that predicted by Eq. (23).

The transient solution to the problem posed by Eq. (24) can be obtained much more easily by making the following transformation:

$$F(r; t) = r^{\alpha} C(r; t) - K \ . \tag{28}$$

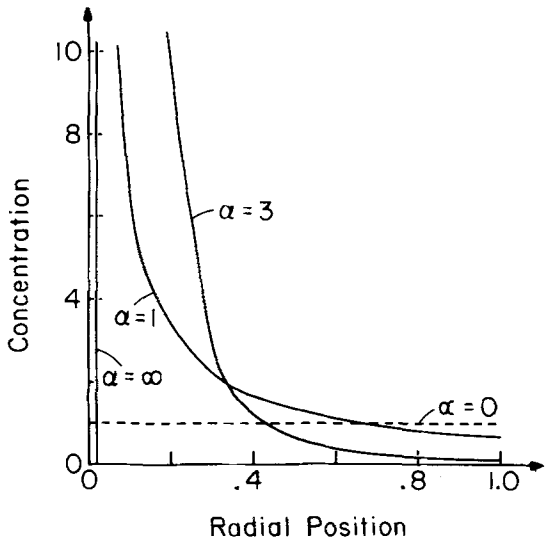


FIG. 3. Predicted steady state concentration profiles for $a = 0.018$ and various values of $\alpha$.

The function $F(r; t)$ satisfies

$$\frac{\partial F}{\partial t} = \frac{\partial^2 F}{\partial r^2} + \frac{(2-\alpha)}{r}\frac{\partial F}{\partial r} , \tag{29}$$

Initial condition at $t = 0$ $\quad F(r; 0) = r^\alpha - K$

Boundary conditions at $r = a$ $\quad \frac{\partial F}{\partial r} = 0$

at $r = 1$ $\quad \frac{\partial F}{\partial r} = 0$

Separated solutions to this problem are easily found and lead to the following results for $F$:

$$F(r; t) = \sum_j A_j e^{-\lambda_j^2 t} r^n [J_{-n+1}(\lambda_j) J_n(\lambda_j r) + J_{n-1}(\lambda_j) J_{-n}(\lambda_j r)] , \tag{30}$$

where $n = \frac{1}{2}(\alpha - 1)$ takes on noninteger values and $J_n$ is the Bessel function of the first kind of order $n$. If $n$ is an integer, then the solution also contains Bessel functions of the second kind. The two boundary conditions determine the eigenvalues, which must satisfy

$$0 = J_{n-1}(\lambda_j a) J_{-n+1}(\lambda_j) - J_{n-1}(\lambda_j) J_{-n+1}(\lambda_j a) . \tag{31}$$

From the orthogonality of the solutions and the initial condition, the coefficients $A_j$ can be found from

$$A_j = \frac{\int_a^1 (r^\alpha - K) r^{(3-\alpha)/2} [J_{-n+1}(\lambda_j) J_n(\lambda_j r) + J_{n-1}(\lambda_j) J_{-n}(\lambda_j r)] dr}{\int_a^1 r [J_{-n+1}(\lambda_j) J_n(\lambda_j r) + J_{n-1}(\lambda_j) J_{-n}(\lambda_j r)]^2 dr} . \tag{32}$$

The transient concentration profile is then given by

$$c(r; t) = K r^{-\alpha} + r^{-\alpha} \sum_j A_j e^{-\lambda_j^2 t} r^n \times [J_{-n+1}(\lambda_j) J_n(\lambda_j r) + J_{n-1}(\lambda_j) J_{-n}(\lambda_j r)] . \tag{33}$$

Figure 4 shows several computed profiles at various times for $\alpha = 2$.

It is important to realize that macromolecular diffusion cannot be neglected for any choice of $\alpha$. If the no-flux boundary conditions are met, then the drift flux at the boundaries must always be in balance with the diffusive flux.

## V. COMPARISON TO EXPERIMENT

Dill and Zimm[3,4] have recently measured the radial concentration profile of DNA produced in a dilute DNA solution confined between rotating concentric cones. The geometric parameters that corresponded to these measurements are

$$\Omega = 2.62 \text{ sec}^{-1} , \quad \theta_0 = 1.332 , \quad \Psi_0 = 1.396$$
$$R_i = 0.05 \text{ cm} , \quad R_0 = 2.77 \text{ cm} , \tag{34a}$$

and the estimated macromolecular parameters are

$$\langle R^2 \rangle_0 = 7.38 \times 10^{-8} \text{ cm}^2 , \quad \tau = 300 \text{ sec} ,$$
$$D = 2.8 \times 10^{-9} \text{ cm}^2/\text{sec} . \tag{34b}$$

The value of $\alpha$ is then approximately $10^6$. The steady state concentration profile [Eq. (26)] predicts nearly total migration of all the solute to the apex of the cones.

Dill and Zimm state that the concentration profiles appear to have reached steady state after several hours of migration. In Fig. 5 we compare the experimental concentration profile reported by them[3,4] after 3.3 h of migration of a $1.25 \times 10^6$ Dalton $T2$ DNA with the results of the present analysis, for the steady state when $\alpha = 2$. The profiles are presented as histograms since concentrations were actually measured by draining equal volume fractions through the apex of the cone. We see that there is in fact quite good qualitative agreement. However, this must be regarded as fortuitous in view of our estimate of what the real value of $\alpha$ is. As Fig. 3 shows, even modestly higher values of $\alpha$ would give unsatisfactory agreement. Of course, it is not entirely certain that the data in Fig. 5 do represent a steady state profile.

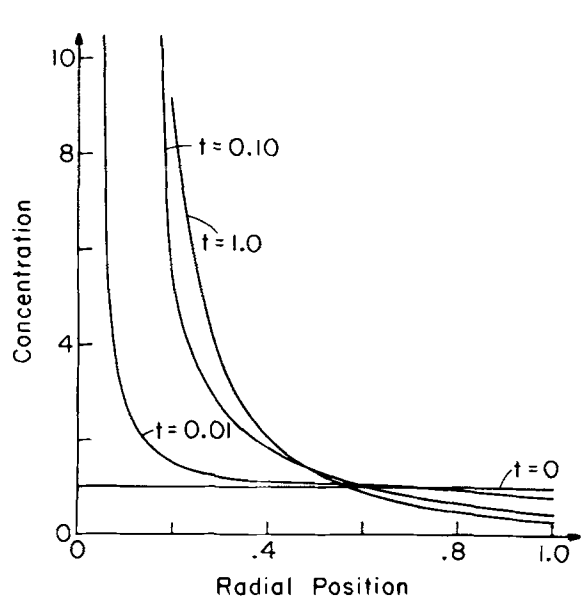


FIG. 4. Transient concentration profiles predicted from the series solution (first four terms) for the case $\alpha = 2$ and $a = 0.018$.

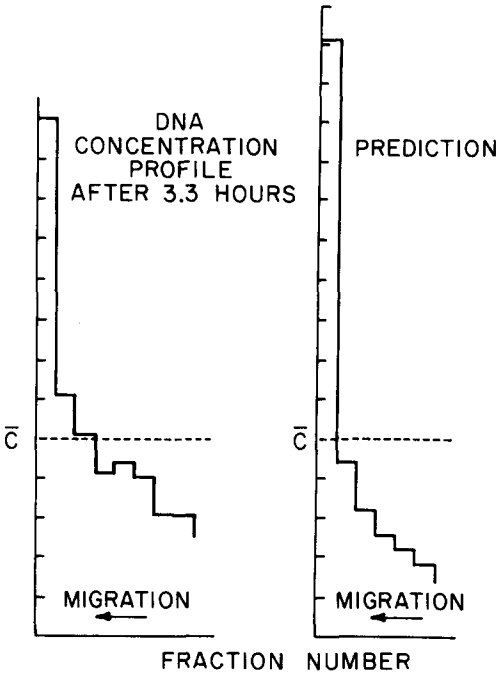


FIG. 5. (a) Experiments of Dill and Zimm (total volume divided into eight equal functions). (b) Steady state prediction for $\alpha = 2$ (total volume divided into six equal fractions).

The transient concentration profiles are formally given by Eq. (33). This equation is not practical to apply to a large realistic value of $\alpha$. A finite-difference numerical scheme was formulated to solve Eq. (24); however, it is unstable for values of $\alpha$ much in excess of $\alpha = 2$. This problem occurs because of the very steep concentration gradients that arise in this particular flow geometry near $r = 0$ and $r = 1$. Since these numerical problems are generated by effects near the boundaries, we can obtain short time information on the shape of the concentration profiles away from the boundaries by essentially ignoring the boundary conditions. It takes some time for the sharp profile created by the no-flux condition at $r = 1$ to sweep across the radius of the cone. We can get information on the concentration profile numerically in the time period before this occurs. Partial profiles computed via this procedure are shown in Fig. 6. We can make short time calculations for the mid-radius range in this way for very high values of $\alpha$. We have illustrated the case of $\alpha = 10^5$ because when these profiles are converted to the discretized versions (as in Fig. 5) actually measured by Dill and Zimm, they give very good agreement with the experimental profiles at those times. A value of $\alpha = 10^6$ greatly overpredicts the concentrations in this range of radial positions at these times. The position of the sharp fall in concentration on the high $r$ side of the profile can be estimated quite accurately from the conservation of mass condition within the gap. The region near $r = 0$ cannot be estimated nearly as accurately but, due to the vanishingly small volume as $r$ becomes small, errors here do not affect the remainder of the concentration profile strongly.

In addition to these computed partial profiles, several time scales can be obtained from the theory and compared to experiment. One time scale that is informative is the time necessary for one macromolecule to migrate from the outer solution boundary to the inner solution boundary under the influence of only the drift velocity (i.e., neglecting diffusion effects). This time is given by

$$\bar{t}^* = \int_{R_0}^{R_i} \frac{dr}{v_{\text{dumbbell}}^{\text{drift}}} \quad . \tag{35}$$

Substituting the expression for the drift velocity [Eq. (23)] and the appropriate geometric and molecular parameters into this equation gives a time of 22 min. This time corresponds to the time it would take the trailing edge of the infinitely sharp concentration profile to migrate to the apex in the absence of center-of-mass Brownian motion of the macromolecules. Dill[3] has solved the first-order partial differential equation (corresponding to the assumption of no Brownian motion) by the method of characteristics and estimated this characteristic time to be 1.5 h. Given that a somewhat different molecular model was used, this discrepancy is not too large.

The time scale necessary to develop the concentration profile *fully* can be obtained by estimating the smallest eigenvalue, which can in turn be obtained by forming the Rayleigh quotient. As discussed in Appendix B, for $\alpha = 10^6$, the estimated smallest eigenvalue is $\lambda_1 = 5.0 \times 10^{-4}$. Hence, the estimated time scale to develope the steady state concentration profile is

$$t^{**} = 1/\lambda_1^2 = 4.0 \times 10^6 \ . \tag{36}$$

The dimensional time that corresponds to this is given by $\bar{t}^{**} = t^{**} R_0^2 / D$ and is an extremely long time ($> 10^{16}$ sec), unattainable in any practical experiment. This long time scale for full development is a direct con-

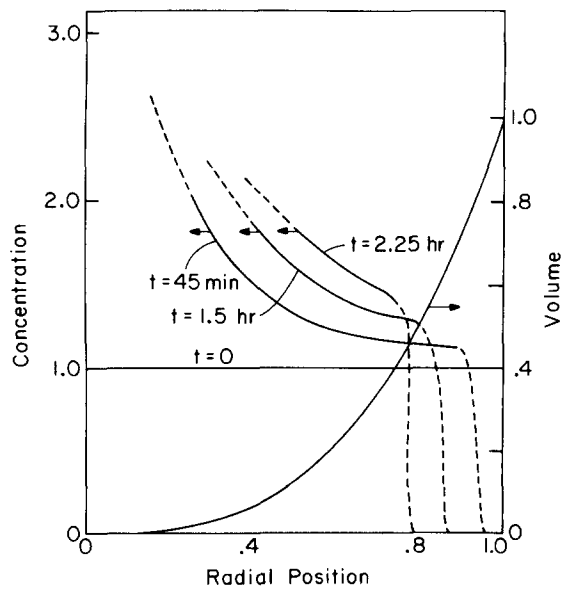


FIG. 6. Partial radial concentration profiles at several times for the case $\alpha = 10^5$. Also plotted is the volume of space between the cones vs position to facilitate transforming to a discrete profile.

sequence of including Brownian motion in the molecular model and of this particular concentric cone geometry, which creates huge concentrations of macromolecules in a vanishingly small volume near the apex.

The picture that emerges from this analysis is that the experimentally observed concentration profiles in the time range of zero to several hours are almost certainly not steady state. Even for small values of $\alpha$ these profiles are very slow to develop. The early stages of this development can be reproduced quantitatively quite well by our model with a value of $\alpha$ somewhat lower than our best estimate of the experimental value. This is due to the infinitely extendable linear elastic dumbbell model we have used and the neglect of hydrodynamic interaction between the beads. These will certainly overpredict the migration effect.

The analysis given by Dill,[3] (neglecting diffusion), gives one characteristic time for the migration and has no nontrivial steady state. Figure 5 shows that for high values of $\alpha$ a very sharp concentration front near the higher $r$ edge, is expected. This feature is consistent with Dill's model. However, the movement of this front is much slower than predicted by Dill's analysis because of the diffusive flux, which is significant near this edge. At the boundaries, the diffusive flux must always be equal to the drift flux.

Quantitative comparisons are of course somewhat out of order since our model assumes infinitely dilute solutions. One criterion of diluteness is that no coil overlap occurs. This may be expressed as

$$c[\eta] \ll 1 , \tag{37}$$

where $[\eta]$ is the intrinsic viscosity of the macromolecular solution. In the Dill and Zimm[3,4] work the solutions at zero time were such that $0.1 < c[\eta] < 1$, so that after some migration occurs, a nondilute region is created where some of the model assumptions are violated. A much more sophisticated theory is required to treat the non-infinitely dilute solution region accurately.

It is interesting to note that the velocity profile given by Eq. (17) is independent of any radial concentration profile. This is because the velocity field is determined solely from the kinematic boundary conditions. However, in the derivation of Eq. (17), a number of assumptions were made. These include the neglect of gravity, inertial effects, and end effects. If these effects are not neglected, a very slow secondary flow is predicted.[10] The secondary flow circulates in the radial direction but is negligible for small rotation rates. Any secondary flow would affect the agreement of this model with experiment. However, the predicted drift velocity would tend to stabilize any secondary flow formed. This stabilizing effect occurs because the drift velocity should increase slightly as the angle $\theta$ is decreased. Since the flow field is nonhomogeneous (the shear rate increases as the angle $\theta$ is decreased) the macromolecular size of interest, $\langle XY \rangle$, should increase slightly as $\theta$ is decreased, and therefore the drift velocity increases with decreasing angle.

The predicted drift velocity [Eq. (23)] is dependent on the macromolecule being anisotropic in the flow field, i.e., a nonzero value of $\langle XY \rangle$. If the macromolecule remained spherically symmetric, then the predicted drift velocity would be zero, since then $\langle XY \rangle = 0$. The predicted drift of a rigid spherical particle in the rotating concentric cone flow is given by Eq. (14) and is found to be zero also. This has been experimentally observed by Highgate and Whorlow,[11] although they did observe a drift velocity when the spheres were suspended in a non-Newtonian fluid. This drift velocity was in the opposite direction, and thought to be caused by normal stresses. Thus, while flexibility is not a requirement for migration, in this geometry, induced or inherent anisotropy is.

## VI. CONCLUSIONS

We have shown that flexible bead-spring type macromolecular models migrate, relative to the undisturbed center of mass solvent velocity, in nonhomogeneous velocity fields. The drift velocity can be calculated explicitly for the dumbbell and Rouse models in general flow fields. These results are analogous to earlier results from continuum mechanics on the motions of neutrally buoyant rigid particles suspended in an arbitrary Stokes flow.[8,12] Under certain simplifications, our results reduce to those. Clearly then, these results have some general validity beyond the apparent limitations of the specific molecular model we have chosen to study. Through the bead-spring models, one might hope to learn more about the motions of deformable particles suspended in viscous media.

An important conclusion one can draw from these results concerns the direction of migration. Drift (meaning center of mass motion relative to local solvent) occurs only *along* streamlines in rectilinear flow; thus, a rectilinear flow, even if nonhomogeneous, will not cause flexible macromolecules to move to where the velocity gradient (and therefore molecular stretching) is minimum, a hypothesis voiced previously.[13,14]

The idea behind that hypothesis is that a macromolecule will attempt to minimize its free energy by moving to where it is minimally stretched. It appears that this quasithermodynamic argument, while appealing, should be abandoned, because there is no mechanism for coupling the intramolecular free energy driving force to a center-of-mass motion (i.e., an intramolecular force can never result in a center-of-mass motion). Other explanations should be sought for the wide range of experimental observations which can be rationalized with this notion.[13–17] We also point out that what we have done here is valid only for unbounded flows. Interactions with solid boundaries need to be examined more closely. Also, particles not having the fore–aft symmetry of the dumbbell may migrate differently.

Macromolecules can migrate across streamlines in curvilinear flows. The viscous forces on the beads drive the model macromolecule to the concave side of the curved streamlines in nonhomogeneous flows. Intramolecular forces from the springs do not cause the center of mass of the bead-spring assembly to move. In every curvilinear flow we have examined, migration of

the dumbbell is dictated by a single parameter $\alpha$, which may be represented by the following relationship:

$$\alpha \sim \frac{\langle R^2 \rangle}{L^2} \frac{v^2 \tau}{D} \tag{38}$$

or

$$\alpha \sim \left(\frac{\langle R^2 \rangle}{L^2}\right)\left(\frac{vL}{D}\right)\left(\frac{v}{L}\tau\right),$$

where $\tau$ is the dumbbell relaxation time, $\zeta/4H$, $L$ is a characteristic length scale for the variation of the velocity gradient, and $v$ is a characteristic flow velocity. The parameters $(vL/D)$ and $(v/L\tau)$ are the Peclet and Weissenberg numbers, respectively.

We have examined in detail the curvilinear flow between concentric cones, since data exist for this flow. Reasonable quantitative agreement with the transient concentration profiles of Dill and Zimm[4] can be obtained if the value of $\alpha$ is adjusted to below the experimental value. Thus the dumbbell overpredicts the migration, due to its infinite extensibility and the neglect of hydrodynamic interaction between the beads. This kind of comparison provides an independent and alternative method to assess the utility and accuracy of various proposed molecular models. Inclusion of center-of-mass Brownian motion is essential to understanding the dynamics of development of these profiles.

We continue working on applying these molecular models in kinematically complex flows of scientific and technological interest.

## ACKNOWLEDGMENTS

The support of the National Science Foundation (DMR-7826629, Polymer Program) and the Research Corporation during the course of this work is gratefully acknowledged.

## APPENDIX A: ANALYSIS OF THE SINGLE-BEAD DISTRIBUTION FUNCTION IN CURVILINEAR FLOWS

Since the mass of the dumbbell is contained solely in the two dumbbell beads, an experimental measurement of concentration may only measure bead concentration. Hence, one might wonder what the continuity equation for bead concentration is. The concentration of beads can be calculated from the configurational distribution function $\Psi(\mathbf{r}_1, \mathbf{r}_2, t)$ by

$$C_b(\mathbf{r}) = \int_{-\infty}^{+\infty}\int_{-\infty}^{+\infty} \Psi(\mathbf{r}_1, \mathbf{r}_2, t) \times [\delta(\mathbf{r}-\mathbf{r}_1)+\delta(\mathbf{r}-\mathbf{r}_2)]\, d\mathbf{r}_1\, d\mathbf{r}_2 , \tag{A1}$$

where $\delta$ is the Dirac delta function. Performing this integration on the six-dimensional continuity equation, Eq. (2), after substitution for $\dot{\mathbf{r}}_1$, and $\dot{\mathbf{r}}_2$ from Eq. (1), yields the following diffusion equation for $C_b(\mathbf{r})$:

$$\frac{\partial C_b}{\partial t} + \nabla\cdot(C_b \mathbf{v}(\mathbf{r})) + \frac{H}{\xi}\nabla\cdot(C_b\langle \mathbf{r}_2 - \mathbf{r}\rangle) = \frac{kT}{\xi}\nabla^2 C_b . \tag{A2}$$

In analogy to Eq. (10), we find

$$\mathbf{J}_b^{nh} = \frac{H}{\xi} C_b(\mathbf{r})\langle \mathbf{r}_2 - \mathbf{r}\rangle . \tag{A3}$$

In the cases where we can estimate the average $\langle \mathbf{r}_2 - \mathbf{r}\rangle$, such as plane Poiseuille flow, we get identical results by using either Eq. (10) or Eq. (A3). No cross-streamline migration is found in rectilinear flow. Circular flows have been examined by this approach. We summarize the results here.

Consider the velocity field given in cylindricial coordinates $(r, \theta, y)$ by

$$\mathbf{v}(r) = r\omega(r)\delta_\theta , \tag{A4}$$

with shear rate equal to

$$\dot{\gamma}(r) = r\frac{d\omega(r)}{dr} . \tag{A5}$$

The configurational distribution function can be expressed in terms of the following variables:

$$\Psi = \Psi(r_1, r_2, \theta, Y, t) , \tag{A6}$$

with $Y = Y_2 - Y_1$ and $\theta = \theta_2 - \theta_1$, since there is angular symmetry and the distribution function is independent of the $Y$ component of the center-of-mass position.

The diffusion equation for the dumbbell in this flow is

$$\frac{\partial \Psi}{\partial t} = (\mathfrak{D} + \mathfrak{R})\Psi, \tag{A7}$$

where $\mathfrak{D}$ and $\mathfrak{R}$ are operators given by

$$\mathfrak{D} \equiv \frac{kT}{\xi}\left(\frac{1}{r_1}\frac{\partial}{\partial r_1}\left(r_1\frac{\partial}{\partial r_1}\right) + \frac{1}{r_1^2}\frac{\partial^2}{\partial\theta^2} + \frac{1}{r_2}\frac{\partial}{\partial r_2}\left(r_2\frac{\partial}{\partial r_2}\right) + \frac{1}{r_2^2}\frac{\partial^2}{\partial\theta^2} + 2\frac{\partial^2}{\partial y^2}\right)$$
$$- \frac{H}{\xi}\left(\frac{1}{r_1}\frac{\partial}{\partial r_1}(r_1[r_2\cos\theta - r_1](\,)) - \frac{1}{r_1}\frac{\partial}{\partial\theta}(r_2\sin\theta(\,))\right)$$
$$+ \frac{H}{\xi}\left(\frac{1}{r_2}\frac{\partial}{\partial r_2}(r_2[r_2 - r_1\cos\theta](\,)) + \frac{1}{r_2}\frac{\partial}{\partial\theta}(r_1\sin\theta(\,))\right) + \frac{2H}{\xi}(\,) + \frac{2H}{\xi} y \frac{\partial}{\partial y}(\,), \tag{A8}$$

$$\mathfrak{R} \equiv [\omega(r_1) - \omega(r_2)]\frac{\partial}{\partial\theta} .$$

Consider now an unbounded solution of dumbbells that have the equilibrium distribution $\Psi_0$ before $t = 0$. At $t = 0$ the velocity field [Eq. (A4)] is imposed throughout the solution and maintained for all times, $t \geq 0$. The time dependent distribution function is given by the solution of Eq. (A7) and, for small times, may be expressed as an expansion in time:

$$\Psi = \Psi_0 + t(\mathfrak{D}+\mathfrak{R})\Psi_0 + \frac{t^2}{2}(\mathfrak{D}+\mathfrak{R})^2\Psi_0 + \frac{t^3}{6}(\mathfrak{D}+\mathfrak{R})^3\Psi_0 + \cdots . \quad \text{(A9)}$$

The equlibrium distribution function is given in cylindrical coordinates by

$$\Psi_0 = N\exp\left[-\left(\frac{H}{2kT}(r_1^2 + r_2^2 - 2r_1 r_2\cos\theta + Y^2)\right)\right], \quad \text{(A10)}$$

where $N$ is a normalization factor. At small time the distribution function can be approximated by retaining only the first few terms of the expansion. The concentration of beads at any radial position $r$ can be obtained from

$$C_b(r) = \int_0^\infty\int_0^\infty\int_0^{2\pi}\int_{-\infty}^{\infty} \Psi\, dY\, d\theta\, [\delta(r-r_1)+\delta(r-r_2)]r_1 \times dr_1 r_2\, dr_2 \equiv \{\Psi\} . \quad \text{(A11)}$$

If this integration is done on Eq. (A9) the following results:

$$C_b(r) = C_{b_0} + \tfrac{1}{6}t^3\{\mathfrak{D}\mathfrak{R}\mathfrak{R}\Psi_0\} + \cdots . \quad \text{(A12)}$$

The initial uniform bead concentration is $C_{b_0}$, and $\{\mathfrak{D}\mathfrak{R}\mathfrak{R}\Psi_0\}$ is

$$\{\mathfrak{D}\mathfrak{R}\mathfrak{R}\Psi_0\} = 2C\frac{\partial}{\partial r}\int_0^\infty r r_1^2[\omega(r_1)-\omega(r)]^2 \times\exp\left(-\frac{H}{2kT}(r_1^2+r^2)\right)I_1\left(\frac{r_1 r H}{kT}\right)dr_1 \quad \text{(A13)}$$

where

$$C = \frac{4\pi H}{\xi}N\sqrt{\frac{2\pi kT}{H}} .$$

$I_1$ is the modified Bessel function of the first kind of order one. This term is exactly equal to zero only for homogeneous flows, since then $\omega(r_1)=\omega(r)=\omega$, a constant. For homogeneous flows no radial bead concentration profile can develop, while for nonhomogeneous flows this term is not in general zero. All of the other terms in Eq. (A9) are zero after the integration is performed. For example, $\{\mathfrak{D}\Psi_0\}$, $\{\mathfrak{D}\mathfrak{D}\Psi_0\}$, $\{\mathfrak{R}\mathfrak{D}\Psi_0\}$, $\{\mathfrak{D}\mathfrak{D}\mathfrak{D}\Psi_0\}$, $\{\mathfrak{D}\mathfrak{R}\mathfrak{D}\Psi_0\}$, and $\{\mathfrak{R}\mathfrak{D}\mathfrak{D}\psi_0\}$ are zero because of the identity $\mathfrak{D}\Psi_0=0$. The term $\{\mathfrak{R}\Psi_0\}$ is zero because of the angular symmetry. The other terms can be shown to be zero after the integrations, except for $\{\mathfrak{D}\mathfrak{R}\mathfrak{R}\Psi_0\}$.

Consider the circular flow given by

$$\omega(r) = \Omega e^{-\alpha r^2} . \quad \text{(A14)}$$

This flow would be difficult to generate, but it demonstrates the principle and makes the integrations simple. For this flow,

$$\{\mathfrak{D}\mathfrak{R}\mathfrak{R}\Psi_0\} = \frac{\partial}{\partial r}\left\{\frac{2C\Omega^2 kT}{H}r^2 e^{-2\alpha r^2} - \frac{16C\Omega^2 H}{kT(4\alpha+2H/kT)^2}r^2\exp\left[r^2\left(-\alpha-\frac{H}{2kT}+\frac{H^2}{k^2T^2(4\alpha+2H/kT)}\right)\right] + \frac{8C\Omega^2 H}{kT(8\alpha+2H/kT)^2}r^2\exp\left(-\frac{H}{2kT}+\frac{H^2}{k^2T^2(8\alpha+2H/kT)}\right)\right\} . \quad \text{(A15)}$$

For an arbitrary choice of $r$, these terms do not cancel. Hence, in this nonhomogeneous flow radial bead concentration profiles do develop in time. We are currently working on the problem of ascertaining whether these profiles persist in the steady state.

The short time solution of the distribution function in a circular flow can be similarly derived in center-of-mass and internal coordinates.

$$\Psi = \Psi(X, Y, Z, Y_c) , \quad \text{(A16)}$$

where $X$, $Y$, and $Z$ are internal coordinates and $Y_c$ is the radial position of the center of mass. The $Y$ direction is taken to be the radial direction and the $X$ direction is taken to be the $\theta$ direction. The equilibrium distribution function is given by

$$\Psi = N\exp\left(-\frac{H}{2kT}(X^2+Y^2+Z^2)\right) . \quad \text{(A17)}$$

The diffusion equation for the dumbbell in a flow with velocity components in the $X$ and $Y$ directions is

$$\frac{\partial\Psi}{\partial t} = (D_{\text{COM}} + R_{\text{COM}})\Psi \quad \text{(A18)}$$

where the operators $D_{\text{COM}}$ and $R_{\text{COM}}$ are given by

$$D_{\text{COM}} \equiv \frac{kT}{\xi}\left(2\frac{\partial^2}{\partial X^2}+2\frac{\partial^2}{\partial Y^2}+2\frac{\partial^2}{\partial Z^2}+\frac{1}{2}\frac{\partial^2}{\partial Y_c^2}\right)+\frac{6H}{\xi}(\,) + \frac{2H}{\xi}X\frac{\partial}{\partial X}+\frac{2H}{\xi}Y\frac{\partial}{\partial Y}+\frac{2H}{\xi}Z\frac{\partial}{\partial Z} \quad \text{(A19)}$$

$$R_{\text{COM}} \equiv -\frac{\partial}{\partial Y_C}[\tfrac{1}{2}(v_{Y_1}+v_{Y_2})(\,)] - \frac{\partial}{\partial X}((v_{X_2}-v_{X_1})(\,)) - \frac{\partial}{\partial Y}[(v_{Y_2}-v_{Y_1})(\,)] .$$

$v_{\alpha i}$ is the velocity at bead $i$ ($i=1, 2$), in direction $\alpha$ ($\alpha = X, Y$). The solution to Eq. (A18) at short times is

$$\Psi = \Psi_0 + t(D_{\text{COM}}+R_{\text{COM}})\Psi_0 + \frac{t^2}{2}(D_{\text{COM}}+R_{\text{COM}})^2\Psi_0 + \cdots . \quad \text{(A20)}$$

From this equation one can calculate the time evolution of center-of-mass radial concentration profiles from

$$C(Y_c) = \iint_{-\infty}^{\infty}\int\Psi(X, Y, Z, Y_c)\,dX\,dY\,dZ \equiv \langle\Psi\rangle . \quad \text{(A21)}$$

Consider now a particular flow field, circular Couette flow, with a velocity field given in terms of center-of-mass position and internal coordinates by[18]

$$\mathbf{v}_i = \left(A_1 Y_c + \frac{A_2}{Y_c}\right)\delta_X + \left(A_1 - \frac{A_2}{Y_c^2}\right) Y\delta_X - \left(A_1 + \frac{A_2}{Y_c^2}\right) X_i \delta_Y + \frac{A_2}{Y_c^3}\left[(Y_i^2 - X_i^2)\,\delta_X + 2X_i Y_i \delta_Y\right] \quad \text{(A22)}$$

$A_1$ and $A_2$ are geometric constants. Calculating the center-of-mass concentration at short times from Eq. (A20) for this flow yields

$$C(Y_c) = C_0 + \tfrac{1}{2} t^2 \langle R_{\mathrm{COM}} R_{\mathrm{COM}} \Psi_0 \rangle + \cdots , \quad \text{(A23)}$$

where, for this particular flow,

$$\langle R_{\mathrm{COM}} R_{\mathrm{COM}} \Psi_0 \rangle = \frac{\pi k^2 T^2}{H^2} N A_2^2 \sqrt{\frac{2\pi kT}{H}} \left\{ \frac{21}{2} \frac{kT}{H} \frac{1}{Y_c^6} - \frac{10}{Y_c^6} \right\} .$$

Radial center-of-mass concentration profiles are seen to develop faster, i.e., at second order in time, than bead concentration profiles, which develop only at third order in time. This conclusion is generally true for any nonhomogeneous flow. We have given a simple illustration here of the flows for which we could do the necessary integrations analytically. This unexpected discrepancy may be important when modeling experimental data and may be responsible for part of the overprediction made by the dumbbell model in comparison with the Dill and Zimm data. This does demonstrate the inherent difference between bead and center-of-mass motion and the problems that may arise when looking only at center-of-mass motion.

## APPENDIX B: ESTIMATION OF THE EIGENVALUES OF (30)

The time necessary to develop fully the steady state concentration profile can be estimated from the smallest eigenvalue, $\lambda_1$, which corresponds to the solution given by Eq. (31). We will start with Eq. (29):

$$\frac{\partial F}{\partial t} = \frac{\partial^2 F}{\partial r^2} + \frac{(2-\alpha)}{r} \frac{\partial F}{\partial r} . \quad \text{(B1)}$$

Initial condition at $t = 0$ $F(r; 0) = r^\alpha - K$

Boundary conditions at $r = a$ $F'(r) = 0$

at $r = 1$ $F'(r) = 0$ .

This equation is separable:

$$\frac{g'}{g} = -\lambda^2 , \quad \frac{f''}{f} + \frac{(2-\alpha)}{r} \frac{f'}{f} = -\lambda^2 , \quad \text{(B2)}$$

where $F(r; t) = f(r)g(t)$. Eigenvalues are determined by

$$r^2 f'' + (2-\alpha) r f' = -\lambda^2 r^2 f \quad \text{(B3)}$$

Boundary conditions at $r = a$ $f' = 0$

at $r = 1$ $f' = 0$ .

This equation can be transformed to

$$(r^{2-\alpha} f')' = -\lambda^2 r^{2-\alpha} f . \quad \text{(B4)}$$

If this equation is multiplied by $f$ and integrated from $a$ to 1, the following results:

$$\int_a^1 [r^{2-\alpha} f']' f \, dr = -\lambda^2 \int_a^1 r^{2-\alpha} f^2 \, dr . \quad \text{(B5)}$$

Integrating the left-hand side by parts and applying the boundary conditions yields

$$\lambda^2 = \frac{\int_a^1 r^{2-\alpha} (f')^2 \, dr}{\int_a^1 r^{2-\alpha} f^2 \, dr} . \quad \text{(B6)}$$

This is known as the Rayleigh quotient.[19] The important characteristic of this quotient is that the minimum of this quotient over the class of functions that satisfy the boundary conditions is the lowest eigenvalue. Hence, an estimate of the lowest eigenvalue can be obtained by making a good guess of an approximate function that satisfies the boundary conditions.

A possible function, $f(r)$, which satisfies both boundary conditions and has the correct qualitative behavior is

$$f(r) = ar - \tfrac{1}{2} a r^2 - \tfrac{1}{2} r^2 + \tfrac{1}{3} r^3 . \quad \text{(B7)}$$

For the case $\alpha = 2$ and $a = 0.018$, Eq. (B6) gives $\lambda_1 = 3.360$, while the exact minimum eigenvalue is $\lambda_1 = 3.199$. For the case $\alpha = 10^6$ and $a = 0.018$, Eq. (B6) gives as the estimated minimum eigenvalue, $\lambda_1 = 5.0 \times 10^{-4}$.


[1] R. B. Bird, O. Hassager, R. C. Armstrong, and C. F. Curtiss, *Dynamics of Polymeric Liquids*, Vol. II: *Kinetic Theory* (Wiley, New York, 1977).
[2] J. H. Aubert and M. Tirrell, J. Chem. Phys. **72**, 2694 (1980).
[3] K. A. Dill, Biophys. Chem. **10**, 327 (1979).
[4] K. A. Dill and B. H. Zimm, Nucleic Acids Research **7**, 735 (1979).
[5] P. J. Flory, *Principles of Polymer Chemistry* (Cornell University, Ithaca, 1953).
[6] A. B. Metzner, in *Improved Oil Recovery by Surfactant and Polymer Flooding*, edited by D. O. Shah and R. S. Schecter (Academic, New York, 1977).
[7] M. Tirrell and M. F. Malone, J. Polym. Sci. Polym. Phys. Ed., **15**, 1569 (1977).
[8] H. Brenner, Chem. Eng. Sci. **21**, 97 (1966).
[9] Throughout this paper we use the notation $\delta_i$ to indicate a unit vector in the coordinate direction $i$.
[10] K. Walters and N. D. Waters, in *Polymer Systems—Deformation and Flow*, edited by R. E. Wetton and R. W. Whorlow (MacMillan, London, 1968), p. 211.
[11] D. J. Highgate and R. W. Whorlow, in Ref. 10, p. 251.
[12] H. Faxen, Arkiv. Mat. Astron. Fys. **20**, 8 (1972).
[13] G. Astarita, G. Marrucci, and G. Balumbo, IEC Fundamentals **3**, 333 (1964).
[14] W. Kozicki, S. N. Pasari, A. R. K. Rao, and C. Tiu, Chem. Eng. Sci. **25**, 41 (1970).
[15] A. J. McHugh, E. Ejike, and C. A. Silebi, Polym. Eng. Sci. **19**, 414 (1979).
[16] A. Geller and W. R. Schowalter, paper presented at Society of Rheology meeting, Boston, October, 1979.
[17] A. B. Metzner, Y. Cohen, and C. Rangel-Nafaile, J. Non-Newtonian Fluid Mech. **5**, 449 (1979).
[18] L. G. Leal, J. NonNewtonian Fluid Mech. **5**, 33 (1979).
[19] C. C. Lin and L. A. Segel, *Mathematics Applied to Deterministic Problems in the Natural Sciences* (MacMillan, New York, 1974).